Journal of Geodesy (2018) 92:779–796
https://doi.org/10.1007/s00190-017-1094-y

ORIGINAL ARTICLE

Precise and efficient evaluation of gravimetric quantities at arbitrarily scattered points in space

Kamen G. Ivanov[1] · **Nikolaos K. Pavlis**[2] · **Pencho Petrushev**[3]

Received: 16 May 2017 / Accepted: 23 November 2017 / Published online: 7 December 2017

Abstract
Gravimetric quantities are commonly represented in terms of high degree surface or solid spherical harmonics. After EGM2008, such expansions routinely extend to spherical harmonic degree 2190, which makes the computation of gravimetric quantities at a large number of arbitrarily scattered points in space using harmonic synthesis, a very computationally demanding process. We present here the development of an algorithm and its associated software for the efficient and precise evaluation of gravimetric quantities, represented in high degree solid spherical harmonics, at arbitrarily scattered points in the space exterior to the surface of the Earth. The new algorithm is based on representation of the quantities of interest in solid ellipsoidal harmonics and application of the tensor product trigonometric *needlets*. A FORTRAN implementation of this algorithm has been developed and extensively tested. The capabilities of the code are demonstrated using as examples the disturbing potential T, height anomaly ζ, gravity anomaly Δg, gravity disturbance δg, north–south deflection of the vertical ξ, east–west deflection of the vertical η, and the second radial derivative T_{rr} of the disturbing potential. After a pre-computational step that takes between 1 and 2 h per quantity, the current version of the software is capable of computing on a standard PC each of these quantities in the range from the surface of the Earth up to 544 km above that surface at speeds between 20,000 and 40,000 point evaluations per second, depending on the gravimetric quantity being evaluated, while the relative error does not exceed 10^{-6} and the memory (RAM) use is 9.3 GB.

Keywords Solid spherical harmonics · Ellipsoidal harmonics · Evaluation at scattered points · Needlets · Fast computation

1 Introduction

Global gravitational models (GGM) are mathematical approximations of the external gravitational potential of an attracting body, like the Earth. It is essential that such models would permit the rigorous evaluation of quantities related to that potential (gravimetric quantities), anywhere on or above the surface of the body, given the position of the evaluation point (Pavlis 2011). Although geodesists have variously considered and studied the representation of the gravitational potential using point masses (Sünkel 1981, 1983), finite element methods (Meissl 1981; Baker 1988) and splines (Sünkel 1984; Jekeli 2005), these approaches have seen only limited application in the representation of (especially) the "static" (i.e., the time-averaged) gravitational field of the Earth. Spherical harmonic functions have prevailed as the standard form used for the representation of the gravitational potential globally, from the very early days of global determinations, to the present. Indeed, the set of coefficients of a spherical harmonic expansion of the gravitational potential has become pretty much synonymous to a GGM.

The evaluation of model-implied gravimetric quantities at points residing over certain geometric surfaces, like the surface of a sphere or of an ellipsoid of revolution, can be done efficiently, even for large number of points, by interpolating from a pre-computed grid of these quantities. The

Approved for public release, 17-477.

✉ Pencho Petrushev
pencho@math.sc.edu

Kamen G. Ivanov
kamen@math.bas.bg

Nikolaos K. Pavlis
Nikolaos.K.Pavlis@nga.mil

[1] Institute of Mathematics and Informatics, Bulgarian Academy of Sciences, 1113 Sofia, Bulgaria

[2] National Geospatial-Intelligence Agency (NGA), Research Directorate (R), Springfield, VA 22150, USA

[3] Department of Mathematics, University of South Carolina, Columbia, SC 29208, USA

formation of the required grid can be done very efficiently, using computational methods like those of Rizos (1979) and Colombo (1981). However, the computation of model-implied gravimetric quantities over a large number of points that are randomly scattered in the 3-dimensional space on or above the surface of the Earth is considerably more complicated, essentially due to the fact that the radial distances of such points vary randomly. There are several types of applications requiring the evaluation of various gravimetric quantities from a high resolution GGM, over large numbers of points that are randomly scattered in 3-dimensional space. Such point sets may be located on or close to the Earth's topography, on the trajectory of an airplane or a missile, or on the orbit of an artificial satellite. The gravimetric quantities required over such point sets depend on the particular application and include height anomalies, gravity anomalies, gravity disturbances, deflections of the vertical, and one or more of the components of the gravitational tensor. Although such evaluation can be done rigorously using point-wise harmonic synthesis (Holmes and Pavlis 2008), this requires significant computational effort, especially when the maximum degree and order of the gravitational model is very high (e.g., exceeds 2000), as is the case after the development and release of the EGM2008 model that extends to degree 2190 (Pavlis et al. 2012).

To address this problem, Rapp (1997) used a Taylor series approach, truncated to the linear gradient term, which was deemed adequate for gravitational models complete to degree and order 360. Hirt (2012) used Taylor expansion up to order 3, Hirt and Kuhn (2012) increased the order to 6, while Balmino at al. (2012) studied the Taylor expansion up to order 60. Bucha and Janák (2014) also studied the expansion up to high orders and presented software for spherical harmonic synthesis at points residing "horizontally" over regular grids (latitude, longitude), whose "vertical" coordinate traces an irregular surface (e.g., the topography). Their publicly available software implements the algorithms developed by Fukushima (2012) for the numerical computation of spherical harmonics of arbitrary degree and order by extending the exponent of floating point numbers and is independent of the harmonic synthesis code that Holmes and Pavlis (2008) also made publicly available, thus enabling inter-comparison of results. Hirt et al. (2016) used the Bucha and Janák (2014) software for expansions to degree and order 21,600, over a regular horizontal grid that traces vertically the topography. Moazezi et al. (2016) presented another approach for fast and efficient synthesis over randomly scattered points, both horizontally and vertically. Eshagh and Abdollahzadeh (2010) presented a semi-vectorization technique for harmonic analysis and synthesis of gravity gradient values residing on regular grids on the sphere. Eshagh and Abdollahzadeh (2012) also presented the irregular semi-vectorization technique for the efficient synthesis of gravity gradients on an elevation model (i.e., again over a regular horizontal grid that traces vertically the topography). In these papers, the evaluation points are located at (irregular) surfaces approximating the Earth's topography, which actually reduces the evaluation to a combination as Taylor series of a few 2-dimensional problems.

There are several other methods, known as 'non-equispaced FFT', for fast evaluation at many points on a sphere of quantities represented in surface spherical harmonics using their coefficients. For example, such methods are developed in (Mohlenkamp 1999; Kunis and Potts 2003; Reuter et al. 2009; Seljebotn 2012; Tygert 2010). For more details, see the introduction in (Ivanov and Petrushev 2015).

This article presents an alternative approach to address the problem of precise and efficient evaluation of model-implied gravimetric quantities over a large number of points that are randomly scattered in the 3-dimensional space on or above the surface of the Earth, from a GGM that extends to very high degree. Our approach was developed with economy of computer memory usage, as well as computational speed in mind, and was tested in the evaluation of the following gravimetric quantities:

- Disturbing potential T
- Height anomaly ζ
- Gravity anomaly Δg
- Gravity disturbance δg
- North–south deflection of the vertical ξ
- East–west deflection of the vertical η
- Second radial derivative of the disturbing potential T_{rr}.

In future versions of our software, we may include additional gravimetric quantities (e.g., the elements of the full gravitational tensor) as well as quantities related to the Earth's magnetic field.

In global gravitational models like EGM2008 (Pavlis et al. 2012), all these gravimetric quantities are represented in solid spherical harmonics extending to degree 2190. Note that most of these quantities are not harmonic functions but can be represented as the product of a slowly varying smooth function κ and a high degree harmonic function F (or a sum of such products). More explicitly, we are interested in fast evaluation of quantities G that can be represented in geocentric spherical coordinates (r, θ, λ), where r is geocentric radial distance, θ is the geocentric colatitude (90^0 minus geocentric latitude), and λ is longitude, in the form:

$$G(r, \theta, \lambda) = \kappa(r, \theta) F(r, \theta, \lambda), \tag{1}$$

where

$$F(r,\theta,\lambda) = \sum_{n=0}^{N} \left(\frac{a}{r}\right)^{n+1} \times \sum_{m=0}^{n} \left(\bar{a}_{nm}\cos m\lambda + \bar{b}_{nm}\sin m\lambda\right) \bar{P}_{nm}(\cos\theta) \qquad (2)$$

and $\kappa(r,\theta)$ is an easy to compute smooth function, which means that $\kappa(r,\theta)$ can be approximated with high accuracy (e.g., 10^{-9}) from low-degree (e.g., degree ≤ 10) solid spherical harmonics. Here $N = 2190$, a is a scaling factor associated with the coefficients $\{\bar{a}_{nm}, \bar{b}_{nm}\}$ that is usually chosen to be numerically equal to the semimajor axis of the adopted reference ellipsoid, $\{\bar{P}_{nm}\}$ are the fully normalized associated Legendre functions, and $\{\bar{a}_{nm}, \bar{b}_{nm}\}$ are known coefficients. Recall that

$$\bar{P}_{nm}(x) = q_{nm}(1-x^2)^{m/2}\frac{d^m}{dx^m}P_n(x),$$

where P_n is the usual nth degree Legendre polynomial and

$$q_{n0} = \sqrt{2n+1};$$
$$q_{nm} = \sqrt{2(2n+1)\frac{(n-m)!}{(n+m)!}}, \quad m = 1,\ldots,n.$$

The **problem** comes down to fast evaluation of products $\kappa(r,\theta)F(r,\theta,\lambda)$ as in (1)–(2) given the coefficients $\{\bar{a}_{nm}, \bar{b}_{nm}\}$ of $F(r,\theta,\lambda)$ at arbitrary (scattered) points in the space on or above the surface of the Earth with prescribed precision, measured as relative or absolute error.

There is a more or less "standard" algorithm that is utilized by the HARMONIC_SYNTH software (Holmes and Pavlis 2008) and made available by NGA at http://earth-info.nga.mil/GandG/wgs84/gravitymod/new_egm/new_egm.html and whose function is documented in http://earth-info.nga.mil/GandG/wgs84/gravitymod/new_egm/README.txt. This method proceeds by computing directly the values of the quantity of interest from its spherical harmonic coefficients by utilization of three term recurrences in stable directions for computing the values of the associated Legendre functions at many points. Here the difficulty stems from the fact that there are very few stable algorithms for accurate evaluation of the associated Legendre functions and all of them have to overcome underflow or overflow for degrees above 1000 or so (the HARMONIC_SYNTH software can handle expansions of degree and order up to 2700). A big advantage of this method over other methods is that it can be applied for evaluation of quantities represented in surface or solid spherical harmonics. Its main drawback is that it is very slow and practically unusable for evaluation at many scattered points. For instance, its implementation on a regular PC computes at most 50 values per second. This means that it takes an hour to compute 180,000 values.

Our goal is to develop an accurate stable algorithm for evaluation of gravimetric quantities at arbitrary scattered points in the space above the surface of the Earth that can perform at the highest possible speed. The presumption is that each gravimetric quantity of interest will be evaluated *many times* at *many (millions) points*. To achieve this, we propose here a method that proceeds in two steps:

Step 1 Given a function $G(r,\theta,\lambda)$ as in (1)–(2) with its coefficients $\{\bar{a}_{nm}, \bar{b}_{nm}\}$ it evaluates G at all points of regular grids $\mathcal{X}_j$ on a carefully selected family of confocal ellipsoids with the first ellipsoid positioned just under the geoid and the rest at certain distances above the geoid (see e.g., Tables 3 and 4).

Step 2 Given the values of G on regular grids $\mathcal{X}_j$ on these confocal ellipsoids, it evaluates G at arbitrary (scattered) points in the external space with prescribed accuracy.

For Step 1 we first convert representation (2) from solid spherical harmonics to solid ellipsoidal harmonics and then use the "standard" harmonic synthesis algorithm in combination with fast Fourier transform (FFT). This method is sufficiently efficient when computing the values of quantities at regular grid points. Step 1 is a pre-computational step that is done once and for all and the computational time for its execution is not so critical.

Our realization of Step 2 relies on the application of *tensor product trigonometric needlets*. Usually, the term "needlets" is used to denote highly localized band limited kernels on the unit sphere that reproduce spherical harmonics of certain degrees. These are also zonal (radial) functions that have the form of needles, which is the reason for calling them "needlets". For more details, see (Ivanov and Petrushev 2015).

In this article, we utilize products of univariate trigonometric needlets. Our method is based on the fact that ellipsoidal harmonics can naturally be extended as bivariate trigonometric polynomials in ellipsoidal coordinates, see Sect. 3.4.1. The trigonometric needlets are kernels of the form

$$\mathcal{K}_N(x) = 1 + 2\sum_{1\leq n<(1+\tau)N} \phi\left(\frac{n}{N}\right)\cos nx,$$

where ϕ is an infinitely differentiable function on $[0,\infty)$ ($\phi \in C^\infty[0,\infty)$) such that $\phi(t) = 1$ on $[0,1]$ and $\phi(t) = 0$ on $[1+\tau,\infty)$ for some $\tau > 0$. Clearly, the integral operator with kernel $\mathcal{K}_N(x-y)$ reproduces the trigonometric polynomials of degree N (see (25)) and, therefore, tensor products of such kernels reproduce trigonometric polynomials in two variables. Furthermore, after discretization of the respective operator by a cubature formula, using regular grid points,

and truncation (see (27)), it becomes an excellent tool for approximation of bivariate trigonometric polynomials.

The superb localization of the kernels $\mathcal{K}_N(x)$ around $x = 0$ (see (26)) plays a decisive role in the application of the trigonometric needlets to fast evaluation of quantities represented in solid spherical or ellipsoidal harmonics. For a detailed account of trigonometric needlets, we refer the reader to the article (Ivanov and Petrushev 2016), see also Sect. 3.4.1 below.

The value of the quantity G to be evaluated at an arbitrary point in the external space is computed by using tensor product trigonometric needlets at appropriate points on ellipsoids near that point and an appropriate polynomial interpolation in the ellipsoidal surface normal direction. A detailed description of this method is given in Sect. 3 below.

The testing of the software realization of our method shows that it is efficient and practically viable. The pre-computational Step 1 that is executed once for a given gravimetric quantity takes between 54 and 120 min on a standard PC for each of the quantities listed above. After the pre-computation is done, the code is capable of computing these gravimetric quantities in the range from the geoid up to 544 km above that surface at speed between 20,000 and 40,000 point evaluations per second on a standard PC, while the relative error does not exceed 10^{-6} and the memory (RAM) use per quantity is 9.3 gigabytes (GB), see Sect. 6.

The key to the success of our method is the fact that *the desired accuracy can be achieved* by using rather sparse grid points on a limited number of ellipsoids (38 ellipsoids for T and ζ, 53 for Δg and δg, 54 for ξ, and 55 for η and T_{rr}) due to the efficiency of the tensor product trigonometric needlets.

The application of our needlet-based algorithm for fast and precise evaluation of quantities represented in solid spherical harmonics is not limited to gravitational modeling. It can be used with equal success in geomagnetism and other areas where quantities are represented in high-degree spherical or ellipsoidal harmonics.

2 Gravimetric quantities represented in solid spherical harmonics

In this section, we describe in detail the gravimetric quantities that our algorithm and software deal with. All of them will be represented as a product just as in (1)–(2) or a sum of such products. We will also derive nonsingular representations for the deflections of the vertical, which lead to stable algorithms.

2.1 Disturbing potential and height anomaly

We begin with the *disturbing potential* T, which we represent in geocentric spherical coordinates by (see also Pavlis et al. 2012, equation 3)

$$T(r,\theta,\lambda) = \frac{\mathcal{GM}}{a}\sum_{n=2}^{N}\left(\frac{a}{r}\right)^{n+1} \times \sum_{m=0}^{n}(\bar{c}_{nm}\cos m\lambda + \bar{s}_{nm}\sin m\lambda)\,\bar{P}_{nm}(\cos\theta),$$

where $\mathcal{GM}$ is the geocentric gravitational constant (universal gravitational constant times the Earth's mass), a is as in (2), and $\bar{c}_{nm}$, $\bar{s}_{nm}$ are the fully normalized spherical harmonic coefficients of T. The coefficients $\bar{c}_{nm}$, $\bar{s}_{nm}$ are computed from the EGM2008 coefficients of the file `EGM2008_to2190_TideFree`, after subtraction of the even degree zonal terms (to degree 20) of the ellipsoidal (reference) gravitational field, from the corresponding EGM2008 coefficients.

In this case, the product representation (1) takes the form

$$T(r,\theta,\lambda) = \kappa(r,\theta)F(r,\theta,\lambda),$$

where $\kappa(r,\theta) = 1$ and $F(r,\theta,\lambda)$ is as in (2) with coefficients

$$\bar{a}_{nm} = \frac{\mathcal{GM}}{a}\bar{c}_{nm}, \quad \bar{b}_{nm} = \frac{\mathcal{GM}}{a}\bar{s}_{nm}. \tag{3}$$

The *height anomaly* ζ is defined (Heiskanen and Moritz 1967, equation (8–10)) by

$$\zeta = \frac{T}{\gamma},$$

where $\gamma = \gamma(r,\theta)$ is the normal gravity. Thus it has a representation as in (1)–(2) with (3), $\kappa(r,\theta) = 1/\gamma(r,\theta)$ and $F(r,\theta,\lambda) = T(r,\theta,\lambda)$.

2.2 Gravity anomaly and gravity disturbance

The spherically approximated *gravity anomaly* $\Delta g = -\frac{\partial T}{\partial r} - \frac{2}{r}T$ (Heiskanen and Moritz 1967, equation (2-154)) is represented just as in (1)–(2) with $G = \Delta g$ and

$$\kappa(r,\theta) = \frac{a}{r}, \quad \bar{a}_{nm} = \frac{\mathcal{GM}}{a^2}(n-1)\bar{c}_{nm},$$
$$\bar{b}_{nm} = \frac{\mathcal{GM}}{a^2}(n-1)\bar{s}_{nm}.$$

The *gravity disturbance* $\delta g = -\frac{\partial T}{\partial r}$ (Heiskanen and Moritz 1967, equation (2-153)) is also represented as in (1)–(2) with $G = \delta g$ and

$$\kappa(r,\theta)=\frac{a}{r},\quad \bar{a}_{nm}=\frac{\mathcal{GM}}{a^2}(n+1)\bar{c}_{nm},$$
$$\bar{b}_{nm}=\frac{\mathcal{GM}}{a^2}(n+1)\bar{s}_{nm}.$$

2.3 The second radial derivative of the disturbing potential

The *second-order radial derivative of the disturbing potential* $T_{rr}=\dfrac{\partial^2 T}{\partial r^2}$ is also represented as in (1)–(2) with $G=T_{rr}$ and

$$\kappa=\left(\frac{a}{r}\right)^2,\quad \bar{a}_{nm}=\frac{\mathcal{GM}}{a^3}(n+1)(n+2)\bar{c}_{nm},$$
$$\bar{b}_{nm}=\frac{\mathcal{GM}}{a^3}(n+1)(n+2)\bar{s}_{nm}.$$

Note that T_{rr} is the most challenging gravimetric quantity (out of those considered in this article) to evaluate due to its very rich high-frequency content, which is reflected in the fact that its coefficients are amplified by terms proportional to the square of the degree, compared to the corresponding coefficients of the disturbing potential.

We next develop stable representations for the deflections of the vertical that, to the best of our knowledge, are new.

2.4 Stable representations of the north–south deflection of the vertical

The spherically approximated *north–south deflection of the vertical* ξ is defined by $\xi=\dfrac{1}{r\gamma}\dfrac{\partial T}{\partial\theta}$, where as before γ is the normal gravity (see also Heiskanen and Moritz 1967, p 235).

In geodesy, it is common to use the derivative representation

$$(1-x^2)\frac{d\bar{P}_{nm}(x)}{dx}=\sqrt{\frac{(n^2-m^2)(2n+1)}{2n-1}}\bar{P}_{n-1,m}(x)-nx\bar{P}_{nm}(x),\tag{4}$$

which implies a representation of the form

$$\xi(r,\theta,\lambda)=\kappa(r,\theta)\frac{F_1^\star(r,\theta,\lambda)r+F_2^\star(r,\theta,\lambda)\cos\theta}{\sin\theta}\tag{5}$$

where $\kappa(r,\theta)=\dfrac{a}{r\gamma(r,\theta)}$ and $F_1^\star$, $F_2^\star$ are harmonic expansions. This representation of the singular at the poles function ξ is computationally unstable due to the $\sin\theta$ term in the denominator.

To overcome the above instability, we employ the representations

$$\sqrt{1-x^2}\frac{d\bar{P}_{nm}(x)}{dx}=\frac{\sqrt{(n-m)(n+m+1)}}{2}\bar{P}_{n,m+1}(x)-\frac{\sqrt{(1+\delta_{0,m-1})(n+m)(n-m+1)}}{2}\bar{P}_{n,m-1}(x),\quad 1\le m\le n;\ n\in\mathbb{N};\tag{6}$$

$$\sqrt{1-x^2}\frac{d\bar{P}_{n0}(x)}{dx}=\sqrt{\frac{n(n+1)}{2}}\bar{P}_{n,1}(x),\ n\in\mathbb{N};\tag{7}$$

where $\delta_{k,\ell}$ is the Kronecker symbol, that is $\delta_{k,\ell}=0$ if $k\neq\ell$ and $\delta_{k,\ell}=1$ if $k=\ell$. These identities are derived from recurrences (15), (17), (19) in (Erdelyi et al. 1953, §3.8). In the geophysics literature, representations (6)–(7) are sometimes attributed to (Bosch 2000) or to (Eshagh 2008, Eq. 18).

Identities (6)–(7) along with the standard formulas

$$\begin{aligned}\cos m\lambda&=\cos(m\pm1)\lambda\cos\lambda\pm\sin(m\pm1)\lambda\sin\lambda,\\ \sin m\lambda&=\sin(m\pm1)\lambda\cos\lambda\mp\cos(m\pm1)\lambda\sin\lambda,\end{aligned}\tag{8}$$

lead to the representation

$$\xi(r,\theta,\lambda)=\kappa(r,\theta)\left(F_1(r,\theta,\lambda)\cos\lambda+F_2(r,\theta,\lambda)\sin\lambda\right),\tag{9}$$

where for $j=1,2$

$$F_j(r,\theta,\lambda)=\frac{\mathcal{GM}}{a^2}\sum_{n=2}^{N}\left(\frac{a}{r}\right)^{n+1}\times\sum_{m=0}^{n}\left(c_{nm}^j\cos m\lambda+s_{nm}^j\sin m\lambda\right)\bar{P}_{nm}(\cos\theta)\tag{10}$$

and $\kappa(r,\theta)$ is as above; the coefficients c_{nm}^j, s_{nm}^j, $j=1,2$, are given in Table 1. Representation (9)–(10) could also be derived after some manipulations from the nonsingular representations of the first Cartesian derivatives of the disturbing potential, see e.g. (Petrovskaya and Vershkov 2012, Eq. (15)).

Observe that the singularity of ξ in representation (9) is contained only in the two multipliers $\cos\lambda$ and $\sin\lambda$, that is, (9) has better numerical stability near the poles than (5). More precisely, our algorithm produces an approximation $\tilde{\xi}$ to ξ, which obeys the same error bound at all points belonging to the same ellipsoid as shown in Sect. 3.5. When the evaluation point coincides with one of the poles (where ξ has a bounded discontinuity), then $\tilde{\xi}$ approximates the latitude limit of ξ with the same precision as at the other points, i.e.,

Table 1 Coefficients in representation (9)–(10) of the north–south deflection of the vertical

$$c^1_{n,m} = \begin{cases} \frac{1}{\sqrt{2}}\sqrt{n(n+1)}\bar{c}_{n,1}, & \text{for } m = 0; \\ \frac{1}{2}\sqrt{(n-1)(n+2)}\bar{c}_{n,2} - \frac{1}{\sqrt{2}}\sqrt{n(n+1)}\bar{c}_{n,0}, & \text{for } m = 1; \\ \frac{1}{2}\sqrt{(n-m)(n+m+1)}\bar{c}_{n,m+1} - \frac{1}{2}\sqrt{(n-m+1)(n+m)}\bar{c}_{n,m-1}, & \text{for } 2 \le m \le n; \end{cases}$$

$$s^1_{n,m} = \begin{cases} 0, & \text{for } m = 0; \\ \frac{1}{2}\sqrt{(n-1)(n+2)}\bar{s}_{n,2}, & \text{for } m = 1; \\ \frac{1}{2}\sqrt{(n-m)(n+m+1)}\bar{s}_{n,m+1} - \frac{1}{2}\sqrt{(n-m+1)(n+m)}\bar{s}_{n,m-1}, & \text{for } 2 \le m \le n; \end{cases}$$

$$c^2_{n,m} = \begin{cases} \frac{1}{\sqrt{2}}\sqrt{n(n+1)}\bar{s}_{n,1}, & \text{for } m = 0; \\ \frac{1}{2}\sqrt{(n-1)(n+2)}\bar{s}_{n,2}, & \text{for } m = 1; \\ \frac{1}{2}\sqrt{(n-m)(n+m+1)}\bar{s}_{n,m+1} + \frac{1}{2}\sqrt{(n-m+1)(n+m)}\bar{s}_{n,m-1}, & \text{for } 2 \le m \le n; \end{cases}$$

$$s^2_{n,m} = \begin{cases} 0, & \text{for } m = 0; \\ -\frac{1}{2}\sqrt{(n-1)(n+2)}\bar{c}_{n,2} - \frac{1}{\sqrt{2}}\sqrt{n(n+1)}\bar{c}_{n,0}, & \text{for } m = 1; \\ -\frac{1}{2}\sqrt{(n-m)(n+m+1)}\bar{c}_{n,m+1} - \frac{1}{2}\sqrt{(n-m+1)(n+m)}\bar{c}_{n,m-1}, & \text{for } 2 \le m \le n. \end{cases}$$

$$\tilde{\xi}(r,0,\lambda) \approx \lim_{\theta\to 0}\xi(r,\theta,\lambda) = \frac{\mathcal{GM}}{\sqrt{2}ar\gamma(r,0)}\sum_{n=2}^{N}\left(\frac{a}{r}\right)^{n+1} \times\sqrt{n(n+1)(2n+1)}[\bar{c}_{n,1}\cos\lambda + \bar{s}_{n,1}\sin\lambda], \tag{11}$$

$$\tilde{\xi}(r,\pi,\lambda) \approx \lim_{\theta\to \pi}\xi(r,\theta,\lambda) = \frac{-\mathcal{GM}}{\sqrt{2}ar\gamma(r,\pi)}\sum_{n=2}^{N}\left(-\frac{a}{r}\right)^{n+1} \times\sqrt{n(n+1)(2n+1)}[\bar{c}_{n,1}\cos\lambda + \bar{s}_{n,1}\sin\lambda], \tag{12}$$

as the values of the limits follow from (9), (10) and the coefficients with $m = 0$ in Table 1.

2.5 Stable representations of the east–west deflection of the vertical

The spherically approximated *east–west deflection of the vertical* $\eta = -\dfrac{1}{r\gamma\sin\theta}\dfrac{\partial T}{\partial\lambda}$ can be represented (see also, Heiskanen and Moritz 1967, p 235) by

$$\eta(r,\theta,\lambda) = \frac{\mathcal{GM}}{ar\gamma(r,\theta)}\sum_{n=2}^{N}\sum_{m=1}^{n}\left(\frac{a}{r}\right)^{n+1} \times m\frac{\bar{P}_{nm}(\cos\theta)}{\sin\theta}[\bar{c}_{n,m}\sin m\lambda - \bar{s}_{n,m}\cos m\lambda],$$

where as above $\gamma = \gamma(r,\theta)$ is the normal gravity. The main drawback of this representation is the $\sin\theta$ term in the denominator, which generates computational instability around the poles—the singularities of η.

We propose the use of the following identity (derived from recurrences (13), (14) in Erdelyi et al. 1953, §3.8)

$$m\frac{\bar{P}_{nm}(x)}{\sqrt{1-x^2}} = \frac{1}{2}\sqrt{\frac{2n+1}{2n-1}}\left(\sqrt{(n-m-1)(n-m)}\,\bar{P}_{n-1,m+1}(x) + \sqrt{(1+\delta_{1,m})(n+m-1)(n+m)}\,\bar{P}_{n-1,m-1}(x)\right), \quad 1 \le m \le n, \tag{13}$$

with $x = \cos\theta$. In the geophysics literature, representations (13) are sometimes attributed to (Eshagh 2008, Eq. 26). Replacing (13) in the above representation of η and using (8) we arrive at the representation

$$\eta(r,\theta,\lambda) = \kappa(r,\theta)\,(F_1(r,\theta,\lambda)\cos\lambda + F_2(r,\theta,\lambda)\sin\lambda) \tag{14}$$

with

$$\kappa(r,\theta) = \frac{a^2}{r^2\gamma(r,\theta)}.$$

Here the functions F_j, $j = 1, 2$, are harmonic and have the representation

$$F_j(r,\theta,\lambda) = \frac{\mathcal{GM}}{2a^2}\sum_{n=1}^{N-1}\left(\frac{a}{r}\right)^{n+1}\sqrt{\frac{2n+3}{2n+1}} \times\sum_{m=0}^{n}\left(c^j_{nm}\cos m\lambda + s^j_{nm}\sin m\lambda\right)\bar{P}_{nm}(\cos\theta), \tag{15}$$

where the coefficients $c^j_{n,m}$, $s^j_{n,m}$, $j = 1, 2$, are given in Table 2. Representation (14)–(15) could also be derived from the nonsingular representations of the first Cartesian derivatives of the disturbing potential, see e.g. (Petrovskaya and Vershkov 2012, Eq. (15)).

Our code gives an approximation $\tilde{\eta}$ to η, which obeys the same error bound over any of the confocal ellipsoids as shown in Sect. 3.5. When the evaluation point coincides with one

Table 2 Coefficients in representation (14)–(15) of the east–west deflection of the vertical

$$c^1_{n,m} = \begin{cases} -\sqrt{2(n+1)(n+2)}\bar{s}_{n+1,1}, & \text{for } m = 0; \\ -\sqrt{(n+2)(n+3)}\bar{s}_{n+1,2}, & \text{for } m = 1; \\ -\sqrt{(n+m+1)(n+m+2)}\bar{s}_{n+1,m+1} - \sqrt{(n-m+1)(n-m+2)}\bar{s}_{n+1,m-1}, & \text{for } 2 \le m \le n; \end{cases}$$

$$s^1_{n,m} = \begin{cases} 0, & \text{for } m = 0; \\ \sqrt{(n+2)(n+3)}\bar{c}_{n+1,2}, & \text{for } m = 1; \\ \sqrt{(n+m+1)(n+m+2)}\bar{c}_{n+1,m+1} + \sqrt{(n-m+1)(n-m+2)}\bar{c}_{n+1,m-1}, & \text{for } 2 \le m \le n; \end{cases}$$

$$c^2_{n,m} = \begin{cases} \sqrt{2(n+1)(n+2)}\bar{c}_{n+1,1}, & \text{for } m = 0; \\ \sqrt{(n+2)(n+3)}\bar{c}_{n+1,2}, & \text{for } m = 1; \\ \sqrt{(n+m+1)(n+m+2)}\bar{c}_{n+1,m+1} - \sqrt{(n-m+1)(n-m+2)}\bar{c}_{n+1,m-1}, & \text{for } 2 \le m \le n; \end{cases}$$

$$s^2_{n,m} = \begin{cases} 0, & \text{for } m = 0; \\ \sqrt{(n+2)(n+3)}\bar{s}_{n+1,2}, & \text{for } m = 1; \\ \sqrt{(n+m+1)(n+m+2)}\bar{s}_{n+1,m+1} - \sqrt{(n-m+1)(n-m+2)}\bar{s}_{n+1,m-1}, & \text{for } 2 \le m \le n. \end{cases}$$

of the poles (where η has a bounded discontinuity), then $\tilde{\eta}$ approximates the latitude limit of η with the same precision as at the other points, i.e.,

$$\tilde{\eta}(r,0,\lambda) \approx \lim_{\theta\to 0}\eta(r,\theta,\lambda) = \frac{\mathcal{GM}}{\sqrt{2}ar\gamma(r,0)}\sum_{n=2}^{N}\left(\frac{a}{r}\right)^{n+1} \times\sqrt{n(n+1)(2n+1)}[\bar{c}_{n,1}\sin\lambda - \bar{s}_{n,1}\cos\lambda], \tag{16}$$

$$\tilde{\eta}(r,\pi,\lambda) \approx \lim_{\theta\to \pi}\eta(r,\theta,\lambda) = \frac{\mathcal{GM}}{\sqrt{2}ar\gamma(r,\pi)}\sum_{n=2}^{N}\left(-\frac{a}{r}\right)^{n+1} \times\sqrt{n(n+1)(2n+1)}[\bar{c}_{n,1}\sin\lambda - \bar{s}_{n,1}\cos\lambda], \tag{17}$$

as the values of the limits follow from (14), (15) and the coefficients with $m = 0$ in Table 2.

3 Theoretical underpinning of our evaluation algorithm

In this section, we describe the main components of our algorithm for fast and accurate evaluation of gravimetric quantities represented in terms of high-degree (> 2000) solid spherical or ellipsoidal harmonics at many arbitrarily scattered points in the space on or above the physical surface of the Earth.

As was alluded to in Sect. 2, all gravimetric quantities of interest to us are represented as a product of the form

$$\begin{aligned} &G(r,\theta,\lambda) = \kappa(r,\theta)F(r,\theta,\lambda) \quad \text{or} \\ &G(r,\theta,\lambda) = \kappa(r,\theta)\left(F_1(r,\theta,\lambda)\cos\lambda + F_2(r,\theta,\lambda)\sin\lambda\right), \end{aligned} \tag{18}$$

where κ is a slowly varying smooth function whose values are easy to compute and F is a harmonic function represented in terms of high-degree solid spherical harmonics as in (2) with given coefficients, that is,

$$F(r,\theta,\lambda) = \sum_{n=0}^{N}\sum_{m=0}^{n}\left(\frac{a}{r}\right)^{n+1} \times(\bar{a}_{nm}\cos m\lambda + \bar{b}_{nm}\sin m\lambda)\bar{P}_{nm}(\cos\theta). \tag{19}$$

Thus it boils down to developing an algorithm for fast and accurate evaluation of harmonic functions $F(r,\theta,\lambda)$ (or $F_1(r,\theta,\lambda)\cos\lambda + F_2(r,\theta,\lambda)\sin\lambda$) as above, multiplied by a very smooth function, at arbitrary points in the space on and above the physical surface of the Earth. Overall, the main difficulty here stems from the fact that this is a 3-*d* problem.

As already presented in the introduction, the main requirement on our algorithm is that the evaluation be *fast*, with *guaranteed accuracy* and with *reasonable use of computer memory* (RAM), so that the algorithm could ideally be implemented in hand-held devices that may have limited computational capabilities. The overriding objective is that one should be able to use the software implementation of our algorithm for evaluation of a given gravimetric quantity at millions of points in near-real time.

We next present the main idea of our method and then elaborate on its building blocks. The simple idea of our algorithm consists of the following steps:

(1) We first convert the spherical harmonic representation of $F(r,\theta,\lambda)$ (or $F_1(r,\theta,\lambda)$ and $F_2(r,\theta,\lambda)$) to the corresponding ellipsoidal harmonic representation, which allows to achieve better approximation error bound (see Sect. 3.1). Of course, if the ellipsoidal harmonic representation of these functions is readily available, the current step can be skipped.
(2) Second, we use the ellipsoidal harmonic coefficients of F and the easy to compute representation of κ to precompute the values of G on regular grids $\mathcal{X}_j$ on carefully selected family of confocal ellipsoids $E_0, E_1, \ldots, E_M$ with increasing semiminor axes and E_0 being just under the geoid (see Sects. 3.2 and 3.3).
(3) We compute the approximate value of G at an arbitrary point x in the external space by using the pre-computed

values of G at appropriate grid points near x. To this end, we use tensor product needlets over appropriate ellipsoids and a special kind of "polynomial" interpolation in the u-direction (see Sect. 3.4).

Here it is important that, although G is not (in general) harmonic, it can be approximated on ellipsoids with very high precision by bivariate trigonometric polynomials due to the fact that κ can be approximated to very high precision by low degree trigonometric polynomials.

We next focus on the details.

3.1 From spherical harmonic to ellipsoidal harmonic expansions

We first convert the representation of the harmonic function $F(r, \theta, \lambda)$ (or F_1, F_2) (see (19)) from solid spherical harmonics to solid ellipsoidal harmonics expressed in ellipsoidal coordinates (u, φ, λ), where φ is the complement of the reduced latitude and u is the semiminor axis of the confocal ellipsoid. These coordinates are related to the spherical coordinates (r, θ, λ) by (see also Heiskanen and Moritz 1967 section 1-19)

$$\begin{cases} r\sin\theta\cos\lambda &= \sqrt{u^2+E^2}\sin\varphi\cos\lambda, \\ r\sin\theta\sin\lambda &= \sqrt{u^2+E^2}\sin\varphi\sin\lambda, \\ r\cos\theta &= u\cos\varphi. \end{cases}$$

Applying Jekeli's transformation (see Jekeli 1988), we transform the coefficients $\bar{a}_{nm}, \bar{b}_{nm}, 0 \le m \le n, 0 \le n \le N$, to $\bar{a}^{\{ell\}}_{n,m}, \bar{b}^{\{ell\}}_{n,m}, 0 \le m \le n, 0 \le n \le N_1$, so that

$$F(r, \theta, \lambda) = H(u, \varphi, \lambda). \tag{20}$$

The ellipsoidal harmonics expansion of $H(u, \varphi, \lambda)$ takes the form

$$H(u,\varphi,\lambda) = \sum_{n=0}^{N_1}\sum_{m=0}^{n} \frac{\bar{S}_{n,m}\left(\frac{u}{E}\right)}{\bar{S}_{n,m}\left(\frac{b}{E}\right)} \times \left(\bar{a}^{\{ell\}}_{nm}\cos m\lambda + \bar{b}^{\{ell\}}_{nm}\sin m\lambda\right)\bar{P}_{nm}(\cos\varphi), \tag{21}$$

where $\bar{S}_{n,m}$ are Jekeli's functions, b is the semiminor axis of the reference ellipsoid and E is its linear eccentricity. In theory $N_1 = \infty$ but in practice, for $N = 2160$, $N_1 = N + 70$ gives (20) with relative error not exceeding 10^{-20}.

For every fixed u the function $H(u, \varphi, \lambda)$ (or $H_1(u, \varphi, \lambda)\cos\lambda + H_2(u, \varphi, \lambda)\sin\lambda$) is a bivariate trigonometric polynomial of degree N_1 (or $N_1 + 1$) and tensor product needlets can be utilized for its fast evaluation, see Sect. 3.4.1. The reason for switching from spherical harmonic expansions to ellipsoidal harmonic expansions is to guarantee smaller approximation error as explained in Sect. 3.5.

Of course, if the gravitational model used is (originally) available in terms of ellipsoidal harmonic coefficients, the present conversion from spherical to ellipsoidal harmonic coefficients is obviously not needed.

3.2 Change of variable in the *u*-direction

A reasonable requirement is that our evaluation algorithm covers the range (ellipsoidal shell) determined by

$$U_0 \le u \le U_1 \text{ with } U_0 = b - 125\,m \text{ and } U_1 = b + 544,000\,m.$$

Here $u = b$ defines the Earth reference ellipsoid and hence the ellipsoid of semiminor axis $u = b - 125$ m is just bellow the Earth geoid. We set $U_1 = b + 544,000\,m$ to cover, with sufficient margin, satellite missions like GRACE in *Low Earth Orbits*. The possible change of the bounds U_0, U_1 is discussed in Sect. 3.6.1.

We now apply a substitution $u = \mu(s)$ with the function μ satisfying the following conditions: μ is defined on an interval $[-s^*, s^*]$, μ is smooth, $\mu(0) = U_0$, $\mu(\bar{s}) = U_1$ for some $0 < \bar{s} < s^*$, $\mu(s)$ is even, i.e., $\mu(-s) = \mu(s)$, and $\mu(s)$ is increasing in $[0, s^*]$ and with "small" derivatives around $s = 0$. Convenient choices for $\mu(s)$ are

$$\mu(s) = U_0 + \frac{U_1 - U_0}{1 - \cos\bar{s}}(1 - \cos s);$$
$$\mu(s) = U_0 + \frac{U_1 - U_0}{\bar{s}^2}s^2; \quad \mu(s) = U_0 + \frac{U_1 - U_0}{\bar{s}^4}s^4,$$

as the last one is used in the codes `hsynth_init` and `hsynth_fast` described in Sect. 4. Now, instead of $G(u, \varphi, \lambda)$ we consider the function

$$g(s, \varphi, \lambda) = G(\mu(s), \varphi, \lambda), \quad 0 \le \varphi \le \pi,\ 0 \le \lambda < 2\pi,\ 0 \le s \le \bar{s}.$$

Thus the evaluation of G is reduced to evaluation of g.

The purpose of the change of variable $u = \mu(s)$ is twofold:

(i) It gives us a function g with *essentially smaller oscillation* of the ellipsoidal surface normal derivatives than the derivatives of G and at the same time the derivatives of g can be explicitly expressed in terms of the ellipsoidal surface normal derivatives of G.
(ii) The function $g(s, \varphi, \lambda)$ being even in s enables us to only work with values of G on and above the ellipsoid $u = U_0$, which is critical for our evaluation scheme.

The choice of $\mu(s)$ (the third one) in our realization of the algorithm is determined by the fact that this $\mu(s)$ leads to optimal ellipsoidal surface normal derivatives of the gravimetric quantities of interest. Hence, the code will require smaller amount of memory compared to the other two options for $\mu(s)$. For evaluation of other quantities, the selection of $\mu(s)$ can be different.

3.3 Construction of regular grids on confocal ellipsoids and pre-computation

We first introduce a family of confocal ellipsoids $E_0, E_1, \ldots, E_M$, where our regular grids will reside. We will use $2J$ point Lagrange interpolation of g in the s-direction, where $J = 3, 4$ or 5, depending on the smoothness of g. By setting $s_j = jh$, $j = 0, 1, \ldots, M$, where h and M are related by $\mu(s_{M-J-1}) \le U_1 \le \mu(s_{M-J})$, we define the confocal ellipsoids E_j with equations $u = \mu(s_j)$. The selection of h is explained in Sect. 3.4.2. Then the regular grid $\mathcal{X}_j$ on E_j in ellipsoidal coordinates is defined by

$$\mathcal{X}_j = \{(\mu(s_j), \varphi_k, \lambda_\ell)\}, \quad j = 0, \ldots, M, \quad \text{with}$$
$$\varphi_k = \frac{\pi k}{K}, \quad k = 0, 1, \ldots, K,$$
$$\lambda_\ell = \frac{2\pi \ell}{L}, \quad \ell = 0, 1, \ldots, L-1.$$

Here L *must be even* so that the values of the same grid can be used for continuation through the poles. The only requirement imposed on K, L and the maximal degree N is

$$\min\{2K, L\} \ge (2+\tau)N, \tag{22}$$

where the parameter τ is from (24) and N is from (23) in Sect. 3.4.1. N represents the degree of the ellipsoidal harmonic expansion H. In the applications, we usually take $L = 2K$, see e.g., Sect. 4 (1).

The pre-computation step consists of computing $G(\mu(s_j), \varphi_k, \lambda_\ell)$ for $k = 0, 1, \ldots, K$, $\ell = 0, 1, \ldots, L-1$, $j = 0, \ldots, M$. For this, we utilize the stable algorithm for evaluation of quantities represented in spherical harmonics mentioned in the introduction.

After the above preparation, we are ready to describe Step 2 of our algorithm for fast and accurate evaluation of gravimetric quantity G at arbitrary points in the ellipsoidal shell $U_0 \le u \le U_1$.

3.4 Evaluation of gravimetric quantities: the core of the algorithm

As before, let $s_j = jh$ and set $u_j = \mu(s_j)$. Our algorithm will compute an approximation $\tilde{G}(u, \varphi, \lambda)$ to the gravimetric quantity $G(u, \varphi, \lambda)$ at an arbitrary point (u, φ, λ) from the ellipsoidal shell $U_0 \le u \le U_1$.

The computation of $\tilde{G}(u, \varphi, \lambda)$ is carried out as follows:

(1) For $u \in [U_0, U_1]$ find $s \in [s_j, s_{j+1}]$, $j \ge 0$, so that $u = \mu(s)$;
(2) Use tensor product needlets (see Sect. 3.4.1) to compute

$$\tilde{g}(s_i, \varphi, \lambda) := \tilde{G}(u_i, \varphi, \lambda),$$
$$i = j - J + 1, j - J + 2, \ldots, j + J,$$

using the values of G at the regular points from each of these $2J$ ellipsoids;
(3) Use Lagrange interpolation to compute $\tilde{G}(u, \varphi, \lambda) := \tilde{g}(s, \varphi, \lambda)$ using the values $\tilde{g}(s_i, \varphi, \lambda)$, $i = j - J + 1$, $j - J + 2, \ldots, j + J$, computed above.

Note that the choice of $\mu(s)$ as an even function yields $u_{-1} = u_1$, $u_{-2} = u_2$, etc., which allows to only use values of $\tilde{G}(u_j, \varphi, \lambda)$ at points with $u_j \ge U_0$ in the computation of $\tilde{G}(u, \varphi, \lambda)$! In this manner, we avoid derivatives of G at points with coordinate u smaller than U_0. The choice $U_0 = b - 125$ m allows to include in the ellipsoidal shell all points *above the geoid*. The values of $u_0 - b, u_1 - b, \ldots$ that our algorithm uses for computing the height anomaly ζ and the second radial derivative of the disturbing potential T_{rr} are given in Tables 3 and 4, respectively.

We next describe in detail the tensor product trigonometric needlets and the Lagrange interpolation we used above.

3.4.1 Trigonometric needlets

The tensor product trigonometric needlets are developed in (Ivanov and Petrushev 2016) and used for fast computation of gravimetric quantities represented in surface spherical harmonics. Here we describe the basic idea of this method.

The univariate trigonometric needlets are kernels of the form

$$\mathcal{K}_N(x) = 1 + 2 \sum_{1 \le n < (1+\tau)N} \phi\Big(\frac{n}{N}\Big) \cos nx, \tag{23}$$

where ϕ is a cutoff function with the following properties: ϕ is smooth on $[0, \infty)$,

$$\phi(t) = 1,\ t \in [0, 1];\ 0 \le \phi(t) \le 1,\ t \in [1, 1+\tau] \text{ and } \phi(t) = 0,\ t \ge 1 + \tau, \tag{24}$$

for some $\tau > 0$. The point is that: (a) The kernel $\mathcal{K}_N(x)$ reproduces trigonometric polynomials of degree $\le N$, that is, if P is a trigonometric polynomial of degree $\le N$, then

$$P(x) = \frac{1}{2\pi} \int_{-\pi}^{\pi} \mathcal{K}_N(x - y) P(y)\, \mathrm{d}y, \tag{25}$$

Table 3 Ellipsoid semiminor axis heights (in meters) above b for the disturbing potential T and the height anomaly ζ

1	−125.00	11	3,231.83	21	54,013.04	31	283,771.51
2	−124.66	12	4,790.93	22	65,801.13	32	325,598.23
3	−119.63	13	6,839.66	23	79,453.05	33	372,288.83
4	−97.82	14	9,471.84	24	95,170.68	34	424,325.64
5	−39.11	15	12,789.96	25	113,171.59	35	482,245.61
6	84.70	16	16,905.46	26	133,690.70	36	546,649.19
7	309.84	17	21,939.00	27	156,982.22	37	618,211.15
8	680.65	18	28,020.82	28	183,321.92	38	697,693.53
9	1, 249.53	19	35,291.24	29	213,009.85	–	–
10	2, 077.01	20	43,901.22	30	246,373.49	–	–

Table 4 Ellipsoid semiminor axis heights (in meters) above b for the second radial derivative of the disturbing potential T_{rr}

1	−125.00	15	2,967.53	29	49,719.26	43	260,514.30
2	−124.92	16	3,951.00	30	57,298.34	44	287,401.31
3	−123.71	17	5,152.54	31	65,724.38	45	316,474.86
4	−118.48	18	6,602.38	32	75,062.28	46	347,883.08
5	−104.40	19	8,332.82	33	85,380.43	47	381,785.04
6	−74.71	20	10,378.22	34	96,750.82	48	418,351.93
7	−20.72	21	12,775.05	35	109,249.38	49	457,768.39
8	68.20	22	15,561.95	36	122,956.21	50	500,233.99
9	204.59	23	18,779.76	37	137,955.95	51	545,964.99
10	402.96	24	22,471.61	38	154,338.09	52	595,196.22
11	679.72	25	26,682.95	39	172,197.43	53	648,183.38
12	1, 053.26	26	31,461.65	40	191,634.49	54	705,205.57
13	1, 543.90	27	36,858.13	41	212,756.02	55	766,568.24
14	2, 173.91	28	42,925.41	42	235,675.61	–	–

(b) If ϕ is infinitely smooth ($\phi \in C^\infty(\mathbb{R})$), then $\mathcal{K}_N(x)$ has almost exponential localization: For an arbitrary $\sigma > 0$ there exists a constant $c_\sigma > 0$ such that

$$|\mathcal{K}_N(x)| \le c_\sigma N(1 + N|x|)^{-\sigma}, \quad |x| \le \pi. \tag{26}$$

Extension of harmonic functions in ellipsoidal coordinates

Taking into account that $\bar{P}_{nm}(\cos\varphi)\cos m\lambda$ and $\bar{P}_{nm}(\cos\varphi)\sin m\lambda$ are trigonometric polynomials in φ and λ for $\varphi \in [0, \pi]$, $\lambda \in [0, 2\pi)$, leads to a natural extension of any harmonic function $H(u, \varphi, \lambda)$ as in (21). More explicitly, $H(u, \varphi, \lambda)$ (or $H_1(u, \varphi, \lambda)\cos\lambda + H_2(u, \varphi, \lambda)\sin\lambda$) with u fixed extends at once to a bivariate trigonometric polynomial $f(\varphi, \lambda)$ for $\varphi, \lambda \in \mathbb{R}$ with the following properties: *The polynomial $f(\varphi, \lambda)$ can be expressed in the form*

$$f(\varphi, \lambda) = \sum_{k=-N}^{N} \sum_{\ell=-N}^{N} c_{k\ell} e^{i(k\varphi + \ell\lambda)},$$

where $c_{k\ell}$ are (complex) coefficients. Furthermore,

$$f(-\varphi, \lambda + \pi) = f(\varphi, \lambda) \quad \text{for} \quad \varphi, \lambda \in \mathbb{R}.$$

The above assertion is an important ingredient in the application of tensor product needlets for fast evaluation of harmonic functions.

The bivariate trigonometric polynomial $f(\varphi, \lambda)$ is evaluated at a point (φ, λ) by tensor product trigonometric needlets of the form

$$\tilde{f}(\varphi, \lambda) = \sum_{|\varphi - \varphi_k| \le \delta_1} \sum_{|\lambda - \lambda_\ell| \le \delta_2} \frac{2}{KL} f(\varphi_k, \lambda_\ell) \times \mathcal{K}_1(\varphi - \varphi_k)\mathcal{K}_2(\lambda - \lambda_\ell), \tag{27}$$

where $\mathcal{K}_1$ and $\mathcal{K}_2$ are trigonometric needlet kernels in φ and λ, respectively.

The number of knots $\{\varphi_k\}$ on $[\varphi - \delta_1, \varphi + \delta_1]$ and the number of knots $\{\lambda_\ell\}$ on $[\lambda - \delta_2, \lambda + \delta_2]$ ranges from 26 to 32 (depending on f) for targeted relative accuracy 2×10^{-7}.

In (27) for λ close to 0 or to 2π, we assume that the definition of λ_ℓ from Sect. 3.3 is extended by the same formula for $\ell < 0$ or $\ell \ge L$, which implies the *periodic* extension $f(\varphi, \lambda + 2\pi) = f(\varphi, \lambda)$ of f. Similarly, for φ close to 0 or to π we extend the definition of φ_k from Sect. 3.3 by the same formula for $k < 0$ or $k > K$, which implies the *even semi-periodic* extension $f(-\varphi, \lambda + \pi) = f(\varphi, \lambda)$ in the case

of T, ζ, Δg, δg or T_{rr}, and the *odd semi-periodic* extension $f(-\varphi, \lambda+\pi) = -f(\varphi, \lambda)$ in the case of ξ or η. These extensions do not require evaluation of the polynomial f at new grid points $(\varphi_k, \lambda_\ell)$ whenever L is even!

We next summarize the main properties of the trigonometric needlets:

(a) They are highly localized and, therefore, the needlet algorithm is local. As a result it is a fast computational method.
(b) The superb localization of the needlets makes the method stable and accurate. It also allows to tightly control the approximation error.
(c) The trigonometric needlets are compatible with spherical and ellipsoidal harmonics, which enables us to work with sparser grids and as a result in economical use of memory (RAM).
(d) The compatibility of the trigonometric needlets with ellipsoidal harmonics also allows to improve the accuracy of computation without changing the grid points. More explicitly, to improve the error of approximation of $f(\varphi, \lambda)$ by $\tilde{f}(\varphi, \lambda)$ we only have to enlarge δ_1 and δ_2 in (27) *without changing the grid points*. This is a big advantage over other computational methods, e.g., fixed-degree polynomial or spline interpolation, which require denser grid points.
(e) The trigonometric needlets are easy to implement in ways that result in fast computational algorithms.

We refer the reader to (Ivanov and Petrushev 2016) for a detailed account of trigonometric needlets.

To speed up our algorithm, we apply tensor product trigonometric needlets for evaluation of quantities $G(u, \varphi, \lambda)$ that are not harmonic but are as in (18) the product of a harmonic function $H(u, \varphi, \lambda)$ as in (21) and a smooth slowly varying function $\kappa(u, \varphi)$ for fixed u. The point is that the factor $\kappa(u, \varphi)$ can be well approximated by a very low-degree bivariate trigonometric polynomial which implies practically the same accuracy of needlet computations for G and H whenever $N \geq 50$.

3.4.2 Lagrange interpolation

As already explained in the description of our algorithm above the approximation $\tilde{G}(u, \varphi, \lambda)$ to the gravimetric quantity $G(u, \varphi, \lambda)$ for u from the ellipsoidal shell $U_0 \leq u \leq U_1$ is obtained by interpolating the values of $g(s, \varphi, \lambda) := G(\mu(s), \varphi, \lambda)$ on equispaced knots $\{s_i\}$, which means interpolating G on several confocal ellipsoids.

Let (φ, λ) be fixed and let $s := \mu^{-1}(u) \in [s_j, s_{j+1}]$. If $\tilde{g}(s, \varphi, \lambda)$ is the Lagrange interpolant of $g(s, \varphi, \lambda)$ at the points $s_i = ih$, $i = j - J + 1, j - J + 2, \ldots, j + J$, then the remainder can be expressed as

$$g(s, \varphi, \lambda) - \tilde{g}(s, \varphi, \lambda) = \frac{(s - s_{j-J+1}) \cdots (s - s_{j+J})}{(2J)!} \frac{\partial^{2J} g}{\partial s^{2J}}(z, \varphi, \lambda)$$

for some $z \in (s_{j-J+1}, s_{j+J})$. Hence

$$|g(s, \varphi, \lambda) - \tilde{g}(s, \varphi, \lambda)| \leq \frac{(2J)!}{J!^2 2^{2J}} \left(\frac{h}{2}\right)^{2J} \max_{s \in [s_{j-J+1}, s_{j+J}]} \left\| \frac{\partial^{2J} g}{\partial s^{2J}}(s, \cdot, \cdot) \right\|, \quad (28)$$

where the uniform norm on the partial derivative of g is taken on $\varphi \in [0, \pi]$, $\lambda \in [0, 2\pi)$.

In our algorithm h is chosen so that:

1. The right-hand side of (28) divided by the uniform norm of g for fixed s always to be smaller than 5×10^{-7};
2. $|s_i - \tilde{s}_i| \leq 10^{-11}$ for $i = 0, 1, \ldots, M$, where $\tilde{s}_i = \mu^{-1}(u_i)$ and $u_i = \mu(s_i)$ in the computer arithmetic.

The first condition requires the evaluation of the $2J$ partial derivative of g, which by the chain rule is expressed via the partial derivatives of G and the derivatives of μ. The second condition provides for a small round-off error in the evaluation of $\tilde{g}$. The reasons for the choice of μ are explained in Sect. 3.2. Moreover, the fact that $\mu(s)$ is even allows us to only operate in the right-hand side of (28) with values of the partial derivatives of G at points (u, φ, λ) with $u \geq U_0$. Thus, we avoid the highly oscillatory behavior of $G(u, \varphi, \lambda)$ in the region $u < U_0$.

Note that the above computational scheme represents for fixed φ, λ an approximation of $G(u, \varphi, \lambda)$ at the nonequally spaced points u_j by a $2J - 1$ degree interpolation spline of maximal defect in the variable $\mu^{-1}(u)$.

3.5 Accuracy

For a gravimetric quantity G, G being T, ζ, Δg, δg, ξ, η or T_{rr}, denote by

$$\mathcal{N}(G, \mathbb{E}, u) = \max_{\{(\varphi,\lambda)\}} |G(u, \varphi, \lambda)|$$

its norm on an ellipsoid with semiminor axis u confocal to the reference ellipsoid. Here (u, φ, λ) stand for the ellipsoidal coordinates of a point and the maximum is taken over all $0 \leq \varphi \leq \pi$, $0 \leq \lambda \leq 2\pi$.

For a point P with spherical coordinates $(r_P, \theta_P, \lambda_P)$ and ellipsoidal ones $(u_P, \varphi_P, \lambda_P)$, $U_0 \leq u_P \leq U_1$, we require that our algorithm computes an approximation $\tilde{G}(u_P, \varphi_P, \lambda_P)$ to the gravimetric quantity $G(u_P, \varphi_P, \lambda_P)$ with relative error $\leq 10^{-6}$, i.e.,

Table 5 Norm $\mathcal{N}(G, \mathbb{E}, b+h)$ of the gravimetric quantity G on the ellipsoids with semiminor axis $b+h$ for some heights h

G\height h	km	0	100	200	300	400	500
$\mathcal{N}(T, \mathbb{E}, b+h)$	m^2/s^2	1041.54	945.64	873.39	811.31	755.93	706.09
$\mathcal{N}(\zeta, \mathbb{E}, b+h)$	m	106.49	99.75	95.01	90.97	87.33	84.01
$\mathcal{N}(\Delta g, \mathbb{E}, b+h)$	mGal	989.20	87.39	50.94	35.95	31.40	27.79
$\mathcal{N}(\delta g, \mathbb{E}, b+h)$	mGal	993.45	102.67	68.51	59.96	53.48	48.14
$\mathcal{N}(\xi, \mathbb{E}, b+h)$	arcsec.	126.78	21.72	11.63	7.52	5.87	5.41
$\mathcal{N}(\eta, \mathbb{E}, b+h)$	arcsec.	94.77	15.70	9.95	8.45	7.63	7.09
$\mathcal{N}(T_{rr}, \mathbb{E}, b+h)$	Eötvös	1296.45	10.49	2.39	1.29	0.81	0.55

Table 6 Evaluation accuracy as an absolute error bound

$G\backslash h$	km	0	20	100	200	500
T	m^2/s^2	1.0×10^{-3}	1.0×10^{-3}	9.5×10^{-4}	8.7×10^{-4}	7.1×10^{-4}
ζ	m	1.1×10^{-4}	1.0×10^{-4}	1.0×10^{-4}	9.5×10^{-5}	8.4×10^{-5}
Δg	mGal	9.9×10^{-4}	3.4×10^{-4}	8.7×10^{-5}	5.1×10^{-5}	2.8×10^{-5}
δg	mGal	9.9×10^{-4}	3.5×10^{-4}	1.0×10^{-4}	6.9×10^{-5}	4.8×10^{-5}
ξ	arcsec.	1.3×10^{-4}	5.2×10^{-5}	2.2×10^{-5}	1.2×10^{-5}	5.4×10^{-6}
η	arcsec.	8.6×10^{-5}	4.1×10^{-5}	1.4×10^{-5}	9.6×10^{-6}	7.1×10^{-6}
T_{rr}	Eötvös	1.3×10^{-3}	1.3×10^{-4}	1.0×10^{-5}	2.4×10^{-6}	5.5×10^{-7}

$$\max_{\substack{\{(\varphi_P,\lambda_P)\}\\ U_0\le u_P\le U_1}} \frac{|\tilde{G}(u_P,\varphi_P,\lambda_P) - G(u_P,\varphi_P,\lambda_P)|}{\mathcal{N}(G,\mathbb{E},u_P)} \le 10^{-6}. \tag{29}$$

Note that (29) holds even when G is ξ or η, which are bounded discontinuous functions at the poles.

The relative precision 10^{-6} in (29) is selected to be better than the relative accuracy of the model EGM2008 itself. When the relative accuracy of the gravimetric model is improved then our codes can be easily modified to work with higher accuracy.

Table 5 illustrates the dependance of the norms $\mathcal{N}(G, \mathbb{E}, u)$ on the ellipsoid semiminor axis. Notice the modest decrease of the norms of T and ζ, the faster decrease of the norms of Δg, δg, T_r, ξ and η, and the very fast decrease of the norms of T_{rr}. The decrease of $\mathcal{N}(G, \mathbb{E}, u_P)$ means smaller absolute errors in (29) when u_P increases.

3.5.1 Absolute error

In some instances, it is useful to know how the bound 10^{-6} on the relative error translates into absolute error for various gravimetric quantities at various heights h above the surface of the earth (geoid). The accuracy in absolute units for each of the gravimetric quantities T, ζ, Δg, δg, ξ, η, and T_{rr} is given in Table 6.

In Fig. 1, we demonstrate how the concept of the uniform relative error, implemented into estimate (29), implies the correlation of the discrepancies with the signal. The plot gives the difference between the values of $\tilde{T}_{rr}$ and T_{rr} on a $2^0 \times 2^0$ grid at the Earth's surface in microEötvös units. The essential statistics of the signal T_{rr} in Eötvös are: minimal value $-$ 183.53247, maximal value 259.85623, mean value $-$ 0.25362, standard deviation 20.03877. The mean absolute ratio of the discrepancy and the signal is 2.27×10^{-7} .

3.5.2 Norms on ellipsoids versus norms on spheres

One may avoid the use of ellipsoidal coordinates as described in Sect. 3.1 and work only in spherical coordinates. Then the target error estimate would be

$$\max_{\substack{\{(\theta_P,\lambda_P)\}\\ U_0\le u_P\le U_1}} \frac{|\tilde{G}(r_P,\theta_P,\lambda_P) - G(r_P,\theta_P,\lambda_P)|}{\mathcal{N}(G,\mathbb{S},r_P)} \le 10^{-6}, \tag{30}$$

where $(r_P, \theta_P, \lambda_P)$ and $(u_P, \varphi_P, \lambda_P)$ denote the spherical and the ellipsoidal coordinates of a point P, respectively, and

$$\mathcal{N}(G,\mathbb{S},r) = \max_{\{(\theta,\lambda)\}} |G(r,\theta,\lambda)|$$

denotes the norm of G on the sphere of radius r. Here the maximum is taken over all $0 \le \theta \le \pi$, $0 \le \lambda \le 2\pi$.

The main problem in obtaining error estimate as in (30) is the very high oscillation of G in the domain under the surface of the earth (see dotted red curves in Fig. 2), i.e., whenever $b \le r_P \le a, b \le u_P$. This would lead to the use of larger size of memory (RAM) because more concentric spheres will be

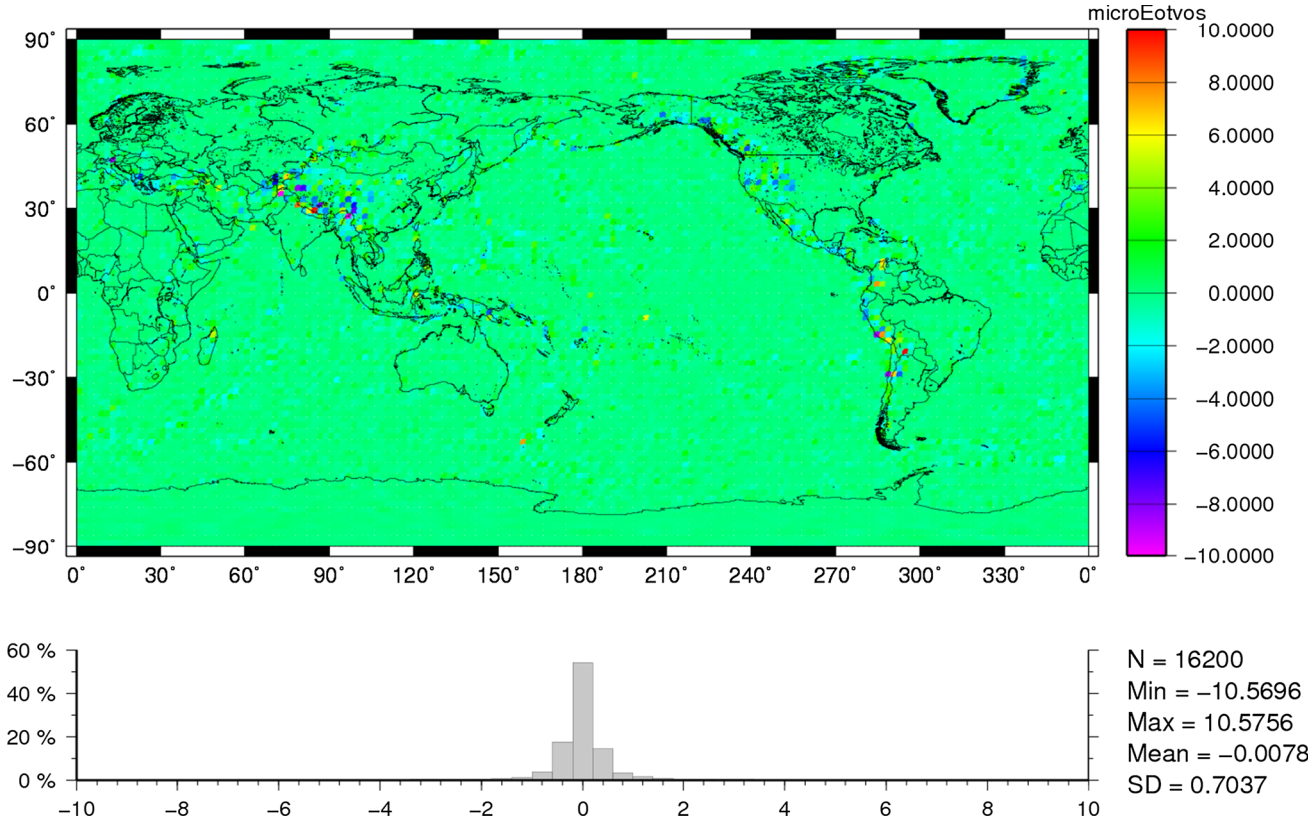

Fig. 1 Values of $\tilde{T}_{rr} - T_{rr}$ on a $2^0 \times 2^0$ grid at the Earth's surface in microEötvös units

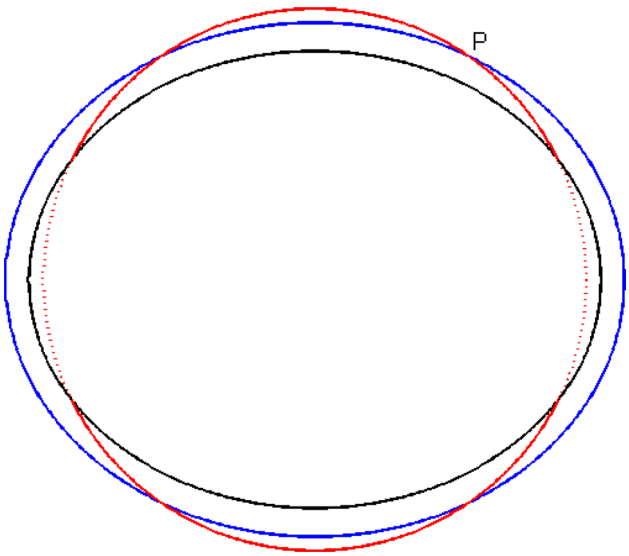

Fig. 2 Point P above the Earth reference ellipsoid (black) congruent to a confocal ellipsoid (blue) and to a sphere (red). Parts of the sphere (dotted red) may be into the reference ellipsoid

needed to get (30) compared with the number of confocal ellipsoids necessary for (29).

Another advantage of the ellipsoidal coordinates over the spherical coordinates here is the fact that $\mathcal{N}(G, \mathbb{S}, r_P)$ could be essentially larger than $\mathcal{N}(G, \mathbb{E}, u_P)$ when the point P is away from the equator as Table 7 shows. This means that estimate (30) could be a lot less precise than estimate (29). Of course, if the point P is on the equator, then the inequality is reversed but the two norms $\mathcal{N}(G, \mathbb{E}, u_P)$ and $\mathcal{N}(G, \mathbb{S}, r_P)$ remain close to each other in this case. Table 7 also shows that the disadvantage of (30) over (29) on the reference ellipsoid is a lot stronger for Δg, δg, ξ, η and T_{rr} than for ζ and T.

The two estimates (29) and (30) become closer with the increase of the point height above the reference ellipsoid. As Table 8 shows the discrepancies at height 20 km for Δg, δg, ξ, η and T_{rr} still exist but they have smaller magnitude, while the discrepancies for ζ and T are practically negligible.

3.6 Discussion

Our algorithm can be applied for scattered point evaluation of an arbitrary quantity G represented as in (18). The factor κ in (18) may also depend on λ, but should be well approximated by low-degree bivariate trigonometric polynomials on every ellipsoid under consideration as explained in Sect. 3.4.1. This would allow a good approximation of G from solid spherical harmonics of slightly larger degree than the degree of F. At the same time, the product κF should satisfy the requirements of Sect. 3.4.2 for an appropriate μ and large enough

Table 7 Ratio of the norms $\mathcal{N}(G, \mathbb{S}, r_P)/\mathcal{N}(G, \mathbb{E}, b)$ for points P on the reference ellipsoid with ellipsoidal coordinates $(b, \varphi_P, \lambda_P)$ and spherical coordinates $(r_P, \theta_P, \lambda_P)$

$G \setminus \varphi_P$	$\pi/2$	$5\pi/12$	$\pi/3$	$\pi/4$	$\pi/6$	$\pi/12$	0
ζ	1.00	1.00	1.00	1.01	1.43	3.03	4.45
Δg	0.93	1.07	1.75	5.70	26.32	83.74	129.19
ξ	0.77	0.90	1.61	6.24	29.25	94.73	146.31
η	0.86	1.00	2.22	9.19	40.64	130.28	202.19
T_{rr}	0.68	0.94	2.59	12.07	58.86	191.90	296.94

The entries for T and δg are not reported because they are very close to the entries for ζ and Δg, respectively

Table 8 Ratio of the norms $\mathcal{N}(G, \mathbb{S}, r_P)/\mathcal{N}(G, \mathbb{E}, b + 20,000)$ for points P 20 km above the reference ellipsoid with ellipsoidal coordinates $(b + 20,000, \varphi_P, \lambda_P)$ and spherical coordinates $(r_P, \theta_P, \lambda_P)$

$G \setminus \varphi_P$	$\pi/2$	$5\pi/12$	$\pi/3$	$\pi/4$	$\pi/6$	$\pi/12$	0
ζ	1.00	1.00	1.00	1.01	1.01	1.02	1.02
Δg	0.93	0.97	1.14	1.47	1.99	2.70	3.10
ξ	0.92	0.94	1.01	1.13	1.33	1.85	2.18
η	0.97	1.00	1.12	1.33	1.61	1.96	2.29
T_{rr}	0.96	1.04	1.34	2.03	3.64	6.81	9.35

The entries for T and δg are not reported because they are very close to the entries for ζ and Δg, respectively

h. Note that the main approximation parameter h heavily depends on the choice of μ and on the coefficients of F and is specific to every gravimetric quantity to be evaluated.

3.6.1 Range of distances above the reference ellipsoid

If one wants to cover areas lying below the ellipsoid of semiminor axis $u = b - 125$ m (e.g., the Dead Sea), then U_0 should be decreased to, say, $U_0 = b - 550$ m. This choice of U_0 would increase the number of ellipsoids from Sect. 3.3 for the range $[U_0, U_1]$ by at most 1 and at the same time preserve the relative error estimate (29). This would result in slightly larger absolute error for the points below the geoid because of the increase of $\mathcal{N}(G, \mathbb{E}, u_P)$ (see Sect. 3.5). Essentially larger decrease of U_0 is not desirable as the discussion in Sect. 3.5.2 indicates.

As was alluded to in Sect. 3.2, the selection $U_1 = b + 544,000\,m$ was made in order to cover satellites in low earth orbits. The simplest way to evaluate gravimetric quantities at points above $b + 544,000$ m is to increase U_1. For example, the choice $U_1 = b + 1,000,000$ m would increase the number of ellipsoids from Sect. 3.3 by 6 for T and ζ and by 8 for the remaining gravimetric quantities, i.e., by approximately 15% (with the same increase of memory and of the time for pre-computing), at the same time preserving the computational speed and the relative error estimate (29). At high altitudes ($u > b + 1,000,000$ m), the gravimetric quantities of interest can be approximated with relative error 10^{-6} by low-degree solid spherical harmonics which allow for good computational speed.

It is important to point out that for all gravimetric quantities, we deal with in this article the step h we use for the range $[b - 125, b + 544,000]$ will ensure the required accuracy of approximation also for the range $[b - 550, b + 1,000,000]$.

Another possible scenario is when one wishes to cover points on or near the Earth's topography only. That means to choose, e.g., $U_1 = b + 10,000$ m. Assume that one wants to compute values of the second radial derivative of the disturbing potential T_{rr}. Then Tabel 4 shows that the current version of our algorithm will use 24 ellipsoids to compute the values of T_{rr} at arbitrary scattered points from this region. The speed and accuracy will be the same as before. This version of our algorithm would be more economical in the size of memory (RAM) used than the current version. Roughly it will use half the RAM. However, if one is interested in covering points on the Earth's topography or on any other surface, then the problem could be considered as a combination of a few 2-dimensional ones and our algorithm can be modified so that the use of RAM would be reduced substantially with the speed and accuracy remaining the same or better.

3.6.2 Regular grids on ellipsoids

From algorithmic point of view, the computation of the values of a gravimetric quantity G at the points of the regular grid $\mathcal{X}_j$ ($j = 0, 1, \ldots, M$) residing on the confocal ellipsoid E_j (see Sect. 3.3) can be performed directly in solid spherical harmonics without passing to ellipsoidal ones as in Sect. 3.1. But from analytic point of view, error estimates as (29) can be guaranteed for needlet approximation only if the *restriction* of G on E_j is approximated within a margin of 10^{-8} by bivariate trigonometric polynomials of degree close to the degree of the original series. As shown in Sect. 3.1, Jekeli's transformation provides such an approximation error (not exceeding 10^{-20}) by increasing the degree from 2190 to 2260. If the ellipsoid eccentricity was larger than the Earth's one or if another type of surface of revolution is used then one may need higher trigonometrical degree for good approximation which will result in a denser grid. For more detailed account of the approximation error when using trigonometric needlets, see (Ivanov and Petrushev 2016).

3.6.3 Needlets versus spline interpolation

Clearly, the role of the trigonometric needlets in the algorithm described in Sect. 3.4 can be played by spline interpolation based on local *high-degree* polynomial Lagrange interpolation. A detailed comparison of these two schemes is given in (Ivanov and Petrushev 2016, §3.5). The overall conclusion

is that if using spline interpolation, in order to guarantee the accuracy and speed we require here, one will be forced to use at least 3.3 times more memory (RAM) for regular grid data than the needlet-based software, that means at least 33 GB rather than 10 GB RAM. Therefore, the needlets have a significant advantage over spline interpolation. One should expect additional slowdown of the computation when using high degree spline interpolation due to stability problems.

Our evaluation algorithm combines two approximation methods: needlet approximation on surfaces (e.g., ellipsoids) and fixed-degree spline interpolation in the normal direction to these surfaces. The spline degrees are 5, 7 or 9 depending on the smoothness of the gravimetric quantity near the boundary—the ellipsoid with $u = U_0$. Here "smoothness" means that the ratio of the norm of the 6th, 8th or 10th derivative and the norm of the gravimetric quantity is essentially smaller than the same ratio for an arbitrary polynomial of degree 2190. Such *low-degree* spline interpolation require prior knowledge of the approximated quantity but gives us the best speed under the reasonable memory usage of under 10 GB for regular grid data.

In case one wants to achieve better accuracy, say 10^{-8}, then the strategies for the two approximation methods are different. For the needlet approximation, one employs the same regular grid (or any other grid satisfying (22)) but uses more nodes. This leads to the same size of memory (per ellipsoid) and slower evaluation speed. In the case of fixed-degree spline approximation, one is forced to decrease the step h in order to guarantee the required accuracy using estimate (28). This implies the same evaluation speed but larger size of memory due to the usage of more ellipsoids.

3.6.4 Ultra-high-degree harmonic expansions

In recent years, spherical harmonics of degree 10,800 or higher have been used in geopotential modeling. Next, we briefly discuss the estimated requirements for using our algorithm for evaluation of such ultra-high-degree harmonic expansions.

The exact number of the necessary confocal ellipsoids will be determined based on the (ultra-high-degree) harmonic expansion coefficients using the criterion of Sect. 3.4.2. This criterion clearly indicates that the number of the needed ellipsoids depends on the smoothness of the harmonic expansion of interest in the radial direction and the targeted accuracy. However, one may expect that the coefficients of degree greater than 2160 decay at a rate similar to the one of the coefficients of degree not exceeding 2160. As a result, the smoothness of the ultra-high-degree harmonic expansion in the radial direction above the surface of the Earth will remain the same. Therefore, if the accuracy remains the same, the number of ellipsoids will be approximately the same. For 5 times higher model degree, there will be 25 times more regular points on every ellipsoid, which means 233 GB memory—currently not possible on desktops. In addition to the 125 times longer work (in double precision arithmetic) of the initialization code, there will be underflow in the grid evaluation and the Fukushima (2012) method (or other extended precision arithmetic) has to be used. At the same time *the accuracy and the speed* of our method after the pre-computation of the necessary grids would be the same! Also the local nature of our algorithm could help to reduce the memory requirements by sorting scattered points by regions.

On the other hand, the "standard" software will work some 25 times slower without counting the underflow that inevitably will occur. The Fukushima (2012) method will additionally slow down the computations. The model coefficient set will also increase 25 times, but this is not so critical memory requirement.

Naturally, any model that uses 10,800 degree spherical harmonics should achieve better approximation than the 2160 degree EGM2008 and then the accuracy of the computation should be higher. Assume that we wish to guarantee 5 times higher accuracy for fast evaluation of gravimetric quantities using some 10,800 degree model than the accuracy for the current EGM2008, that is, the required accuracy is improved from 10^{-6} to 2×10^{-7}, measured as relative error. Then applying the criterion of Sect. 3.4.2 for evaluation, for example, of Δg, δg, ξ or η leads us to the conclusion that our method will require approximately 22% more ellipsoids than the necessary ones for 10^{-6} accuracy and the number of points on every ellipsoid will increase by 6% in each direction; the speed after pre-computation will remain the same.

It should be pointed out that our tensor product trigonometric needlet method would not experience memory problems when applied for evaluation of harmonic expansions of degree up to 15,000 at scattered points on any sphere or ellipsoid. We have successfully tested it on functions represented in spherical/ellipsoidal harmonics of degree 12,960.

3.6.5 Evaluation of very "rough" functions

If our computational method is applied to a very "rough" function (in the radial direction), then the targeted relative accuracy will be achieved if the number of confocal ellipsoids is increased depending on the norms of the derivatives of that quantity.

However, the grid spacing on the ellipsoids could remain the same; it will provide the same accuracy and speed as before. Thus, the relative accuracy 2×10^{-7} of the tensor product trigonometric needlets is always guaranteed (independent of the "roughness" of the trigonometric polynomial) by using 26 knots for $\tau = 1.6$ or 32 knots for $\tau = 1.0$. Note that $\tau = 1.6$ means denser grid than $\tau = 1.0$ and we can achieve the desired accuracy with less knots here. The independence of the grid from the "roughness" of the function

being evaluated is an important advantage of needlet tensor product method over other ones, e.g., fixed-degree polynomial or spline interpolation.

4 Description of software

Software realization in FORTRAN of the algorithms for fast and precise evaluation of quantities represented in terms of solid spherical or ellipsoidal harmonics has been developed. The covered gravimetric quantities are: disturbing potential T (in m^2/s^2), height anomaly ζ (in *meters*), gravity anomaly Δg (in *mGal*), gravity disturbance δg (in *mGal*), north–south deflection of the vertical ξ (in *arcseconds*), east–west deflection of the vertical η (in *arcseconds*), and the second radial derivative of the disturbing potential T_{rr} (in *Eötvös*). In the present implementation, the values of these quantities are derived from the Earth Gravitational Model EGM2008 (Pavlis et al. 2012).

We next provide some basic information about our software.

(1) The program `hsynth_init` precomputes the values of the gravimetric quantity of interest at regular grid points located on confocal ellipsoids as described in Sect. 3.3. The "standard" method for evaluation of *surface* spherical harmonic *gridded* values is applied. The coefficients of the ellipsoidal harmonic expansions are obtained via Jekeli's transformation from the coefficients of the spherical harmonic expansions (see Sect. 3.1), which in turn are derived as explained in Sect. 2 from the EGM2008 coefficients given in file `EGM2008_to2190_TideFree`. The number of confocal ellipsoids is chosen to cover the range $[U_0, U_1]$ with step h, which in turn depends on the evaluated gravimetric quantity as explained in Sect. 3.4.2.
The number of regular grid points located on an ellipsoid is: 4015×8028 for T and ζ ($2.69' \times 2.69'$ grid); 3346×6690 for $\Delta g, \delta g, \xi, \eta$ and T_{rr} ($3.23' \times 3.23'$ grid). The grids are further extended as explained in Sect. 3.4.1.
The number of confocal ellipsoids used by the code is 38 for T and ζ, 53 for Δg and δg, 54 for ξ, 55 for η and T_{rr}. The values of the parameter h generating these ellipsoids are 0.021435478 for T and ζ, 0.015295193 for Δg, 0.015323755 for δg, 0.01510703 for ξ, 0.014712992 for η, 0.01500051 for T_{rr}.
The pre-computed values are not included in the package because of their 9.3 GB sizes. On the computer where the tests were performed, it takes approximately 54 min to run the code for T or ζ, 1 hour for Δg, δg or T_{rr} and 2 hours for ξ or η. The program `hsynth_init` is run once for every gravimetric quantity.

(2) The program `hsynth_fast` is an implementation of the algorithm described in Sect. 3.4 to compute the values of any of the above gravimetric quantities at arbitrarily scattered points in the external space. As input `hsynth_fast` uses the output of `hsynth_init`, which does not depend of the sets of points on which the code `hsynth_fast` is run. The output of `hsynth_init` is used to initialize the program `hsynth_fast` in the same way as the gravitational model coefficients are used to initialize the "standard" synthesis algorithms, e.g., the code `hsynth_standard` described below.

(3) The code `hsynth_standard` was developed for testing the *accuracy* of the main code `hsynth_fast` and is used as a benchmark for its *speed*. Here, the gravimetric quantities are evaluated using the same method implemented in the `harmonic_synth` program (Holmes and Pavlis 2008) for the case of randomly scattered evaluation points, except for the north–south and east–west vertical deflections ξ and η. These are computed here using the more stable numerical methods presented in Sects. 2.4 and 2.5, respectively. Unlike `hsynth_init` and `hsynth_fast`, which use ellipsoidal harmonic coefficients, `hsynth_standard` uses spherical harmonic coefficients to evaluate the gravimetric quantities. In the present implementation, the EGM2008 coefficients were used.

When executed the three codes report some statistics for their work. Among the displayed `hsynth_standard` statistics, one can find the relative errors of the gravimetric quantity computed by `hsynth_fast`. The speed of our realization of the two methods can be compared using the reported numbers "Values per second". In both programs, these numbers represent pure computational time, ignoring the time necessary to read the input or to write the output.

As the speed of the "standard" method (`hsynth_standard`) is approximately 46 values per second for $T, \zeta, \Delta g, \delta g$ and T_{rr} or 23 values per second for ξ and η, it is not advisable to run this code with more than 10,000 points.

5 Software download

The software described above is now open source and is available at the website of the Interdisciplinary Mathematics Institute (IMI), University of South Carolina: http://imi.cas.sc.edu/. To download the source codes in MATLAB and in FORTRAN with its precompiled executables visit http://imi.cas.sc.edu/gravimetric-quantities/.

Table 9 `Values per second` by `hsynth_standard` and `hsynth_ fast` and the improvement in computational speed

Gravimetric quantity	`hsynth_standard`	`hsynth_fast`	Improvement (times)
T	46.50	40884.58	879.24
ζ	46.37	40677.58	877.24
Δg	46.11	24716.76	536.04
δg	46.21	24510.06	530.41
ξ	23.32	24831.27	1064.81
η	46.33	24690.56	532.93
T_{rr}	46.29	19918.77	430.30

A user manual with a detailed description of the software, instructions for its use and test statistics is also available at the IMI website.

6 Comparison with existing methods. Results

The FORTRAN software has been extensively tested on a laptop with 2.4 GHz PC, CPU Intel Core i7 with 16 GB of RAM and 250 GB SSD used to store the input and output files. The `hsynth_fast` uses 11 GB of RAM.

The program `hsynth_fast` has been tested on up to 30,000,000 randomly distributed within the whole shell $[U_0, U_1]$ points, which were processed with the speed indicated in the third column of Table 9. The relative error did not exceed 4.64×10^{-7} for all tests measured with `hsynth_standard`. Recall that the relative error is computed by (29) and some values of the norms $\mathcal{N}(G, \mathbb{E}, u)$ are given in Table 5.

The improvement in computational speed of our code (measured by `Values per second`) to the software using the "standard" method is given in the last column of Table 9. The reciprocals of the entries in the second and third columns multiplied by the number of evaluation points give the "pure synthesis times". They do not include the times for loading the point coordinates and for writing the computed values, which are also proportional to the number of evaluation points. They also do not include the times for initializing the codes—approximately 30 s for loading the grid values by `hsynth_fast` or 11 s for loading the model coefficients by `hsynth_standard`. For more details see the user manual from Sect. 5.

The different entries in the third column of Table 9 reflect the different approximation methods used in `hsynth_fast` to compute the respective gravimetric quantities. The speed for ξ in the second column of Table 9 is twice smaller than for the other quantities because two harmonic expansions (instead of one) are used for its evaluation in `hsynth_standard`. The reported speed for η in the second column of Table 9 is for the "standard" method, which is not stable near the poles. If our stable method is used, then the speed for η is similar to the speed for ξ.

7 Conclusion

The experiments with the software described above clearly demonstrate the capability of our needlet method for fast and stable evaluation of gravimetric quantities represented in terms of *solid* spherical harmonics at scattered points *in space*. After the pre-computational step, the current version of our software (`hsynth_fast`) runs between 430 and 1064 times faster than the software (`hsynth_standard`) that employs "standard" harmonic synthesis methods. This speed allows to use our code for near-real-time calculations on standard computers. It also is capable of evaluation of gravimetric quantities at large number (millions) of points.

Future work Our method for fast and accurate evaluation of quantities represented in solid spherical harmonics is not limited to gravimetric quantities only. It can be successfully used for evaluation of any quantity that is represented in high-degree solid spherical or ellipsoidal harmonics. In particular, it can be utilized for evaluation of the elements of the geomagnetic field in the current Enhanced Magnetic Model (EMM2015), which are represented in terms of spherical harmonics of degree 720, see https://www.ngdc.noaa.gov/geomag/EMM/index.html.

In many areas ranging from geodesy and geomagnetism to cosmology and atmospheric sciences data are collected at accelerating rates with higher and higher resolution and accuracy every year. The assimilation of these data will lead to the development of mathematical models with high accuracy and predictability. The needlet method described in this article has a lot of potential. Since our method is local, it is parallelizable and can be utilized for fast and accurate evaluation of quantities represented in spherical/ellipsoidal harmonics of degree 10,000 or higher. The results reported here indicate that the needlets can be a handy tool in future more accurate models.

Acknowledgements The authors would like to thank the referees for their constructive suggestions for improvements.

References

Baker EM (1988) A finite element model of the Earths anomalous gravitational potential. Report 391, Department of Geodetic Science and Surveying, Ohio State University, Columbus

Balmino G, Vales N, Bonvalot S, Briais A (2012) Spherical harmonic modelling to ultra-high degree of Bouguer and isostatic anomalies. J Geod 86:499–520. https://doi.org/10.1007/s00190-011-0533-4

Bosch W (2000) On the computation of derivatives of Legendre functions. Phys Chem Earth 25:655–659

Bucha B, Janák J (2014) A MATLAB-based graphical user interface program for computing functionals of the geopotential up to ultra-high degrees and orders: geocient computation at irregular surfaces. Comput Geosci 66:219–227. https://doi.org/10.1016/j.cageo.2014.02.005

Colombo OL (1981) Numerical methods for harmonic analysis on the sphere. Report 310, Department of Geodetic Science and Surveying, Ohio State University, Columbus

Erdelyi A, Magnus W, Oberhettinger F, Tricomi FG (1953) Higher transcendental functions, vol I. McGraw-Hill Book Company, New York, Toronto, London

Eshagh M (2008) Non-singular expressions for the vector and the gradient tensor of gravitation in a geocentric spherical frame. Comput Geosci 34(12):1762–1768. https://doi.org/10.1016/j.cageo.2008.02.022

Eshagh M, Abdollahzadeh M (2010) Semi-vectorization: an efficient technique for synthesis and analysis of gravity gradiometry data. Earth Sci Inf 3(3):149–158

Eshagh M, Abdollahzadeh M (2012) Software for generating gravity gradients using a geopotential model based on an irregular semivectorization algorithm. Comput Geosci 39:152–160. https://doi.org/10.1016/j.cageo.2011.06.003

Fukushima T (2012) Numerical computation of spherical harmonics of arbitrary degree and order by extending exponent of floating point numbers. J Geod 86(4):271–285. https://doi.org/10.1007/s00190-011-0519-2

Heiskanen WA, Moritz H (1967) Physical geodesy. Freeman and Company, San Francisco

Hirt C (2012) Efficient and accurate high-degree spherical harmonic synthesis of gravity field functionals at the earth's surface using the gradient approach. J Geod 86(9):729–744. https://doi.org/10.1007/s00190-012-0550-y

Hirt C, Kuhn M (2012) Evaluation of high-degree series expansions of the topographic potential to higher-order powers. J Geophys Res 117:B12407. https://doi.org/10.1029/2012JB009492

Hirt C, Reussner E, Rexer M, Kuhn M (2016) Topographic gravity modelling for global Bouguer maps to degree 2160: validation of spectral and spatial domain forward modelling techniques at the 10 microGal level. J Geophys Res Solid Earth 121:B51763. https://doi.org/10.1002/2016JB013249

Holmes SA, Pavlis NK (2008) A FORTRAN program for very-high-degree harmonic synthesis HARMONIC_SYNTH. http://earth-info.nga.mil/GandG/wgs84/gravitymod/new_egm/new_egm.html

Ivanov KG, Petrushev P (2015) Fast memory efficient evaluation of spherical polynomials at scattered points. Adv Comput Math 41:191–230

Ivanov KG, Petrushev P (2016) Highly effective stable evaluation of bandlimited functions on the sphere. Numer Algorithms 71:585–611

Jekeli C (2005) Spline representations of functions on a sphere for geopotential modeling. Report 475, Department of Civil and Environmental Engineering and Geodetic Science, Ohio State University, Columbus

Jekeli C (1988) The exact transformation between ellipsoidal and spherical harmonic expansions. Manuscr Geod 13:106–113

Kunis S, Potts D (2003) Fast spherical fourier algorithms. J Comput Appl Math 161:75–98

Meissl P (1981) The use of finite elements in physical geodesy. Report 313, Department of Geodetic Science and Surveying, Ohio State University, Columbus

Moazezi S, Zomorrodian H, Siahkoohi HR, Azmoudeh-Ardalan A, Gholami A (2016) Fast ultrahigh-degree global spherical harmonic synthesis on nonequispaced grid points at irregular surfaces. J Geod 90:853–870. https://doi.org/10.1007/s00190-016-0915-8

Mohlenkamp M (1999) A fast transform for spherical harmonics. J Fourier Anal Appl 5:159–184

Pavlis NK (2011) Gravity, global models. In: Gupta HK (Ed.) Encyclopedia of solid earth geophysics, pp 533–547. https://doi.org/10.1007/978-90-481-8702-7_76

Pavlis NK, Holmes SA, Kenyon SC, Factor JK (2012) The development and evaluation of the Earth Gravitational Model 2008 (EGM2008). J Geophys Res 117:B04406. https://doi.org/10.1029/2011JB008916

Petrovskaya MS, Vershkov AN (2012) Spherical harmonic series for derivatives of all orders of the gravitational potential of a planet and their application in satellite geodesy and space navigation. Cosm Res 50:152–159. https://doi.org/10.1134/S001095251201008X

Rapp RH (1997) Use of potential coefficient models for geoid undulation determinations using a spherical harmonic representation of the height anomaly/geoid undulation difference. J Geod 71(5):282–289

Reuter M, Ratner M, Seideman T (2009) A fast method for solving both the time-dependent Schroedinger equation in angular coordinates and its associated 'm-mixing' problem. J Chem Phys 131(094108):1–6

Rizos C (1979) An efficient computer technique for the evaluation of geopotential from spherical harmonic models. Aust J Geod Photogramm Surv 31:161–169

Seljebotn D (2012) Wavemoth-fast spherical harmonic transforms by butterfly matrix compression. Astrophys J Suppl Ser 199(1–5):1–12

Sünkel H (1981) Point mass models and the anomalous gravitational field. Report 328, Department of Geodetic Science and Surveying, Ohio State University, Columbus

Sünkel H (1983) The generation of a mass point model from surface gravity data. Report 353, Department of Geodetic Science and Surveying, Ohio State University, Columbus

Sünkel H (1984) Splines: their equivalence to collocation. Report 357, Department of Geodetic Science and Surveying, Ohio State University, Columbus

Tygert M (2010) Fast algorithms for spherical harmonic expansions, III. J Comput Phys 229:6181–6192